



## Article

# Zircon from diamondiferous kyanite gneisses of the Kokchetav massif: Revealing growth stages using an integrated cathodoluminescence, Raman spectroscopy and electron microprobe approach

Olga V. Rezvukhina<sup>1\*</sup> , Andrey V. Korsakov<sup>1</sup> , Dmitriy I. Rezvukhin<sup>1</sup> , Denis S. Mikhailenko<sup>1,2</sup> ,  
Dmitry A. Zamyatin<sup>3,4</sup> , Evgeny D. Greshnyakov<sup>5</sup> and Vladimir Ya. Shur<sup>5</sup>

<sup>1</sup>Sobolev Institute of Geology and Mineralogy, Siberian Branch of the Russian Academy of Sciences, 3 Koptyuga ave., Novosibirsk, 630090, Russia; <sup>2</sup>Guangzhou Institute of Geochemistry, Chinese Academy of Sciences, 511 Kehua st., Tianhe, Guangzhou, 510640, China; <sup>3</sup>Zavaritsky Institute of Geology and Geochemistry UB RAS, 15 Vonsovskogo st., Ekaterinburg, 620016, Russia; <sup>4</sup>Institute of Physics and Technology, Ural Federal University, 21 Mira st., Ekaterinburg, 620002, Russia; and <sup>5</sup>School of Natural Sciences and Mathematics, Ural Federal University, 51 Lenin Ave., Ekaterinburg, 620000, Russia

### Abstract

Zircon crystals from diamondiferous kyanite gneisses of the Barchi-Kol area (Kokchetav massif, Northern Kazakhstan) have been investigated by a combined application of cathodoluminescence (CL), Raman spectroscopy and electron probe microanalysis (EPMA). The zircon crystals exhibit up to four distinct domains characterised by significantly different CL signatures and parameters of the  $\nu_3(\text{SiO}_4)$  ( $1008\text{ cm}^{-1}$ ) Raman band (i.e. full width at half maximum, position and intensity). Extremely metamict zircon cores (Domain I) host inclusions of low-pressure minerals (quartz and graphite) and the outer mantles (Domain III) are populated by ultrahigh-pressure relicts (diamond and coesite), whereas inner mantles (Domain II) and overgrowth rim zones (Domain IV) are inclusion free. Both the zircon cores and rims have very low Ti concentrations, implying formation temperatures below  $760^\circ\text{C}$ . The Ti content in the inner mantles (up to 40 ppm) is indicative of temperatures in the  $760\text{--}880^\circ\text{C}$  range. The temperature estimates for the outer mantles are  $900\text{--}940^\circ\text{C}$ , indicating a pronounced overlap with the peak metamorphic values yielded by the Zr-in-rutile geothermometer for the same rocks ( $910\text{--}950^\circ\text{C}$ ). The internal textures of the zircons and the occurrence of index minerals within the distinct domains allow us to unravel the stages of the complex metamorphic history recorded in the zircon. Our data show that the zircon cores are inherited seeds of pre-metamorphic (magmatic?) origin, the inner mantles were formed on the prograde metamorphic stage, the outer mantles record ultrahigh-pressure metamorphism and the outermost rims mark the retrograde metamorphic stage. The observed zircon internal textures are thus clearly correlated with distinct growth events, and in some examples reflect a major part of the metamorphic history. It is concluded that the combined application of the CL, Raman spectroscopy and EPMA techniques to zircon offers significant potential for deciphering the metamorphic evolution of deeply-subducted rocks.

**Keywords:** zircon, cathodoluminescence, Raman spectroscopy, electron microprobe, ultrahigh-pressure metamorphism, Kokchetav massif

(Received 26 August 2020; accepted 19 November 2020; Accepted Manuscript published online: 25 November 2020; Associate Editor: Craig Storey)

### Introduction

Ultrahigh-pressure metamorphic (UHPM) rocks of coesite and diamond stability fields have attracted the attention of researchers over the years, as they are unique objects for reconstructing the metamorphic history of subduction-related mineral associations (e.g. Schertl and Sobolev, 2013; Liou *et al.*, 2014). Super-silicic titanite with coesite exsolution (Ogasawara *et al.*, 2002) and  $\text{K}_2\text{O}$ -rich (up to 1.5 wt.%) clinopyroxene (Shimizu, 1971; Sobolev and Shatsky, 1990; Claoué-Long *et al.*, 1991; Zhang

*et al.*, 1997; Katayama *et al.*, 2001; Mikhno and Korsakov, 2013) suggest the host UHPM rocks formed at depths in excess of 200 km (Katayama *et al.*, 2000; Ogasawara *et al.*, 2002; Perchuk *et al.*, 2002; Mikhno and Korsakov, 2015). Subsequent rapid exhumation of these rocks at rates of tens of kilometers per million years is the accepted mechanism for returning the deeply-subducted material to the Earth's surface (Hacker *et al.*, 2003; Dobretsov and Shatsky, 2004; Liao *et al.*, 2018).

Regardless of the profound knowledge of UHPM complexes, many aspects currently remain disputable. An ongoing problem for diamond-bearing complexes is the reconstruction of the prograde metamorphic history, which is usually erased during exhumation as a result of dehydration reactions, diffusion and anatexis. One of the minerals capable of providing insights into the UHPM rock evolution is zircon, which is widespread in UHPM assemblages and is a common host for inclusions of

\*Author for correspondence: Olga V. Rezvukhina, Email: [olgashchepetova@igm.nsc.ru](mailto:olgashchepetova@igm.nsc.ru)

Cite this article: Rezvukhina O.V., Korsakov A.V., Rezvukhin D.I., Mikhailenko D.S., Zamyatin D.A., Greshnyakov E.D. and Shur V.Y.a. (2020) Zircon from diamondiferous kyanite gneisses of the Kokchetav massif: Revealing growth stages using an integrated cathodoluminescence, Raman spectroscopy and electron microprobe approach. *Mineralogical Magazine* 84, 949–958. <https://doi.org/10.1180/mgm.2020.95>

UHP minerals, preventing their phase transition during the exhumation of the geological unit (Sobolev, 1994; Chopin and Sobolev, 1995; Parkinson and Katayama, 1999; Rubatto and Hermann, 2007; Liu and Liou, 2011).

A pioneer attempt to reconstruct the prograde evolution of the diamond-grade Kokchetav rocks was carried out on the basis of an investigation into mineral inclusions in zircon from different lithologies of the Kokchetav massif (Katayama *et al.*, 2000). The combined application of optical microscopy, cathodoluminescence (CL), Raman spectroscopy and electron probe microanalysis (EPMA) of zircon grains revealed their complex internal textures, i.e. the presence of cores with pre-UHP metamorphic inclusions (graphite, quartz, phengite and apatite) and mantles enclosing HP and UHP inclusions (garnet, omphacite, coesite and diamond). This zonal distribution of mineral inclusions in zircon has been interpreted as a prograde PT record of the UHP metamorphic evolution (Katayama *et al.*, 2000).

As the geological evolution of rocks proceeds, the zircon structural state can change to the metamict state characterised by a low order of atom arrangement (Caruba *et al.*, 1985; Chakoumakos *et al.*, 1987; Woodhead *et al.*, 1991). Metamictisation is the process of radiation damaging the zircon structure by the recoil cores and  $\alpha$ -particles formed during the  $\alpha$ -decay of U and Th radionuclides (Murakami *et al.*, 1986; Weber *et al.*, 1997; Ewing *et al.*, 2003). To indicate and estimate the crystallinity degree of the zircon structure, the CL (Vavra, 1990; Hanchar and Miller, 1993; Schaltegger *et al.*, 1999; Nasdala *et al.*, 2002; Campomenosi *et al.*, 2020), back-scattered electron imaging (BSE; Nasdala *et al.*, 2006; Zamyatin *et al.*, 2017, 2019), X-ray absorption (Farges and Calas, 1991) and infrared spectroscopy (Zhang *et al.*, 2000; Zhang and Salje, 2001) techniques have been applied extensively. It has been shown that one of the most suitable *in situ* techniques to measure the metamictisation degree of zircon is Raman spectroscopy (Nasdala *et al.*, 1995; Palenik *et al.*, 2003; Marsellos and Garver, 2010; Campomenosi *et al.*, 2020). The change of zircon crystallinity has been reported to be reflected in downshifting, broadening and decrease of intensity of the  $\nu_3(\text{SiO}_4)$  band that occurs at  $1008\text{ cm}^{-1}$  in the zircon Raman spectrum (Nasdala *et al.*, 2001; Shimizu and Ogasawara, 2014; Campomenosi *et al.*, 2020).

The objective of this study is a combined application of CL, Raman spectroscopy and EPMA techniques to zircon from diamondiferous kyanite gneisses of the Kokchetav massif (Northern Kazakhstan) in order to reveal the metamorphic history encoded within the zircon interiors and rims. The synthesis of these analytical approaches allowed us to identify mineral inclusions in zircon and reconcile their distribution within individual zircon domains. Together with temperature assessments yielded by conventional geothermometers, the obtained data were employed to reconstruct distinct stages of zircon growth throughout the PT record of the host UHPM gneissic assemblages. Our data show that the zircon internal textures revealed clearly correlate with distinct growth events. The combined methodology described here can be reproduced and used for zircon from other UHP complexes the world over.

## Geological outline and sample description

The Kokchetav massif is a mega-mélange zone that consists of a series of units characterised by diverse PT conditions of formation (Dobretsov *et al.*, 1995a,b; 1998; Theunissen *et al.*, 2000; Buslov *et al.*, 2015). The massif is subdivided by the Chaglinka fault

zone into two main blocks (diamond-free Kulet and diamondiferous Kumdy-Kol), which in turn include five terranes: Kumdy-Kol; Barchi-Kol; Enbek-Berlyk; Sulu-Tyube; and Kulet (Fig. 1a) (Dobretsov *et al.*, 2006). The peak metamorphic conditions for the diamond-bearing Kumdy-Kol rocks exceed 4 GPa and  $1100^\circ\text{C}$  (Sobolev and Shatsky, 1990; Shatsky *et al.*, 1991; Dobretsov *et al.*, 1995b; Mikhno and Korsakov, 2015), whereas for the coesite-bearing Kulet rocks the values of  $>3\text{ GPa}$  and  $720\text{--}760^\circ\text{C}$  have been assessed (Shatsky *et al.*, 1998; Ota *et al.*, 2000; Parkinson, 2000; Theunissen *et al.*, 2000). A distinctive feature of the Kokchetav massif is a high mean rate ( $1.8\text{ cm/year}$ ) of rock exhumation (Hacker *et al.*, 2003; Dobretsov *et al.*, 2006), which, in particular, has been considered as a reason for coesite preservation during exhumation (Mosenfelder *et al.*, 2005). The age of the peak metamorphism for the Kokchetav UHPM rocks estimated by U–Pb zircon methods (Claoué-Long *et al.*, 1991; Hermann *et al.*, 2001, 2006; Katayama *et al.*, 2001, 2003; Katayama and Maruyama, 2009; Stepanov *et al.*, 2016b) as well as by Sm–Nd mineral isochrons from the diamond-bearing rocks and associated rocks (Shatsky *et al.*, 1999) is *ca.* 530 Ma.

The diamond-bearing kyanite gneisses investigated (samples B-11-14 and B-16-14) were collected on the south-west extension of the Barchi-Kol terrane (Fig. 1b), described previously by Shatsky *et al.* (2015). The samples have a medium- to coarse-grained texture without obvious foliation. Rock-forming minerals are kyanite, garnet, quartz, phengite, muscovite, biotite, and feldspar. Accessory minerals are graphite, zircon, rutile, apatite, monazite, allanite, dumortierite, tourmaline, siderite, baryte, pyrrhotite and UHP relicts; diamond and coesite. A characteristic feature of these types of rocks is the abundance of diamond inclusions (up to  $20\ \mu\text{m}$ ) in kyanite (Fig. 2a), garnet (Fig. 2b) and zircon (Fig. 2c). Zircon was identified in the samples studied as inclusions in garnet (Fig. 2e,g) and kyanite (Fig. 2h) as well as in the rock matrix (Fig. 2c,d,f). A more detailed petrographic description of the diamondiferous kyanite gneisses from the Barchi-Kol terrane is provided elsewhere (Shatsky *et al.*, 2015; Shchepetova *et al.*, 2017).

## Methods

The rock samples were crushed, and the zircon separated by conventional heavy-mineral separation techniques were then placed in 25 mm diameter epoxy mounts. The zircons were ground to about half their thickness and polished with a diamond paste. The identification of mineral inclusions in zircon was carried out by optical microscopy using an Olympus BX-51 microscope combined with an Olympus COLOR VIEW III camera and by Raman spectroscopy with a confocal Horiba Jobin-Yvon LabRam HR 800 spectrometer at the Analytical Centre for multi-element and isotope research (Sobolev Institute of Geology and Mineralogy SB RAS, Novosibirsk, Russia). Raman imaging of zircon was undertaken using an Alpha300 AR confocal Raman microscope (WITec GmbH, Germany) at the School of Natural Sciences and Mathematics, Ural Federal University, Ekaterinburg, Russia. The acquisition parameters for the Raman imaging are given in Table 1. The determination of Ti concentrations in zircon for the ‘Ti-in-zircon’ geothermometer was performed at the Common Use Centre of the Ural Branch of RAS ‘Geoanalyst’ (Zavaritsky Institute of Geology and Geochemistry UB RAS, Ekaterinburg, Russia) using a Cameca SX100 electron microprobe equipped with five wavelength-dispersive spectrometers. Titanium concentrations were registered simultaneously on four spectrometers for a 400 s acquisition time using PET

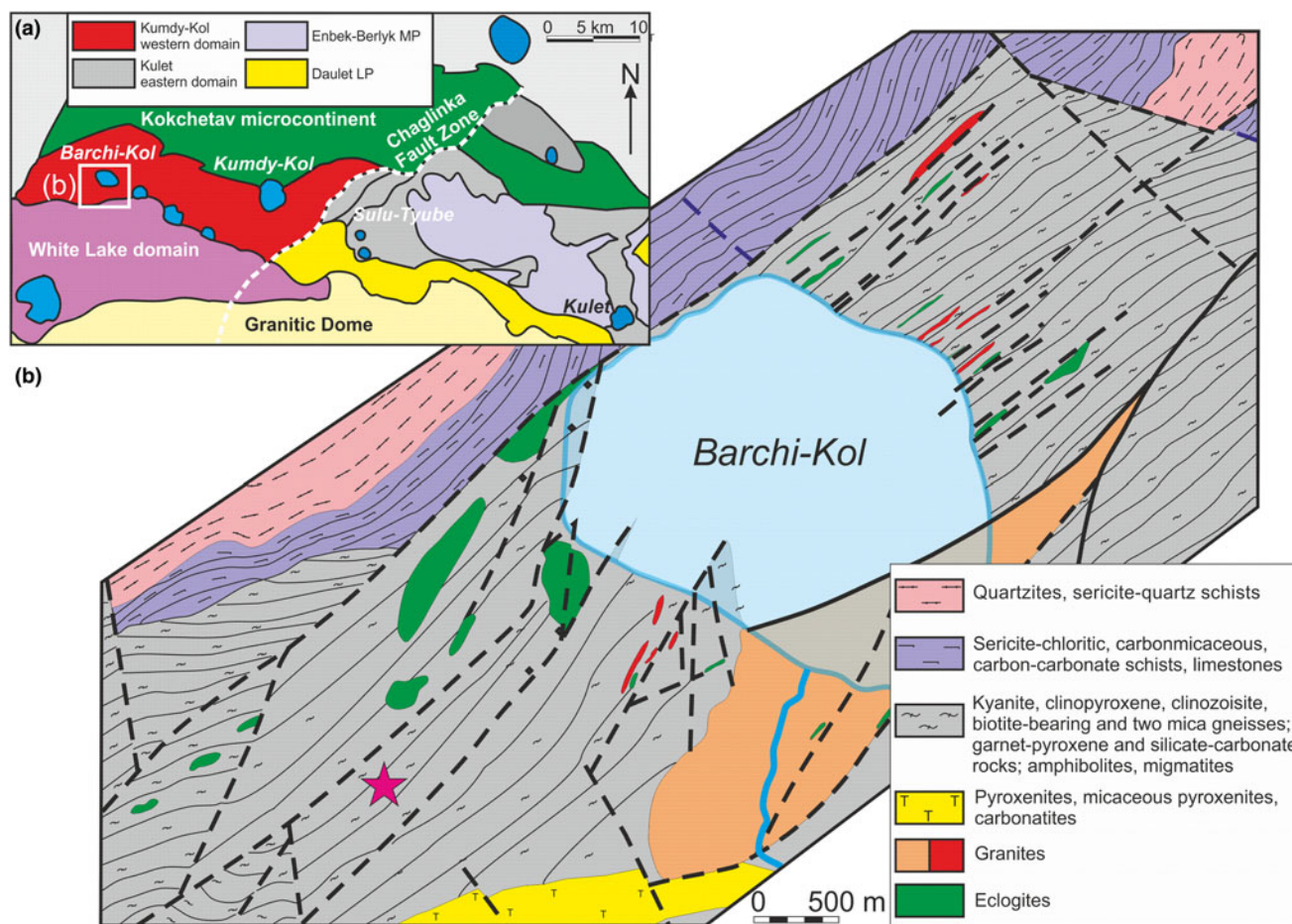


**Fig. 1.** Simplified maps of the Kokchetav massif (a) and Barchi-Kol terrane (b), compiled from Dobretsov and Shatsky (2004) and Korsakov *et al.* (2002), respectively. Magenta star indicates sampling location.

and LPET analysing crystals. Accelerating voltage was 15 kV and sample current was 200 nA. The detection limit of Ti in zircon was 12 ppm. Panchromatic CL-images of zircon were obtained using a Cameca SX100 electron microprobe with a current of 4 nA. The contents of HfO<sub>2</sub>, ThO<sub>2</sub> and UO<sub>2</sub> were measured using a Jeol JXA-8100 electron probe microanalyser at the Analytical Centre for multi-elemental and isotope research SB RAS with a 20 kV accelerating voltage, 200 nA beam current, 2–3 μm beam spot and analysis time 20 s/20 s (peak/background) for HfO<sub>2</sub> and 180 s/180 s for ThO<sub>2</sub> and UO<sub>2</sub>. The detection limits of Hf, U and Th in zircon were 413, 19 and 20 ppm, respectively. To estimate temperature using the 'Zr-in-rutile' geothermometer (Watson *et al.*, 2006; Ferry and Watson, 2007; Tomkins *et al.*, 2007), Zr concentrations in rutile grains derived from the same rock samples were measured using a Jeol JXA-8100 electron probe microanalyser equipped with five wavelength-dispersive spectrometers (accelerating voltage of 20 kV, beam current of 150–200 nA, beam spot of 2–3 μm, and analysis time 180 s/90 s). The detection limit of Zr in rutile was 19 ppm.

## Results

### Zircon characterisation

Zircon from the examined separates occurs as rounded grains 50–200 μm in size. Our combined CL, EPMA and Raman

spectroscopy investigation revealed noticeable internal heterogeneity. In the CL mode, the zircons consist of a series of distinct domains that form 'spotted' zonation (Fig. 3a), or, occasionally, concentric zoning patterns (Fig. 3b–f). A summary of the zircon domain characteristics obtained by the study of 40 grains is provided in Table 2 and a detailed description of each zone is given below.

We have subdivided zircon into four domains, based on their CL signature. Domain I represents rounded zircon cores visible in transmitted light (Fig. 2e). These cores are up to 30 μm in diameter and host inclusions of low-pressure (LP) minerals (graphite and quartz). Occasionally, the zircon cores show oscillatory zoning (Fig. 3e). The cores are commonly surrounded by radial fractures and display low CL intensity (Fig. 3), suggesting a greater degree of metamictisation compared with other domains. The zircon cores can also be distinguished in the Raman maps (Fig. 4) of the  $\nu_3(\text{SiO}_4)$  band by the highest values of the full width at half maximum (FWHM) (15.5–15.7 cm<sup>-1</sup>) (Fig. 4d) and the lowest values of the peak intensities (Fig. 4e,g). The cores have the highest U (up to 1494 ppm) and HfO<sub>2</sub> (up to 2.15 wt.%) concentrations of all the zircon domains, whereas Ti content is below the detection limit (<12 ppm) and Th amounts range up to 115 ppm (Table 2).

Domain II comprises the inner mantles that surround the inherited cores. These inner mantles are devoid of inclusions

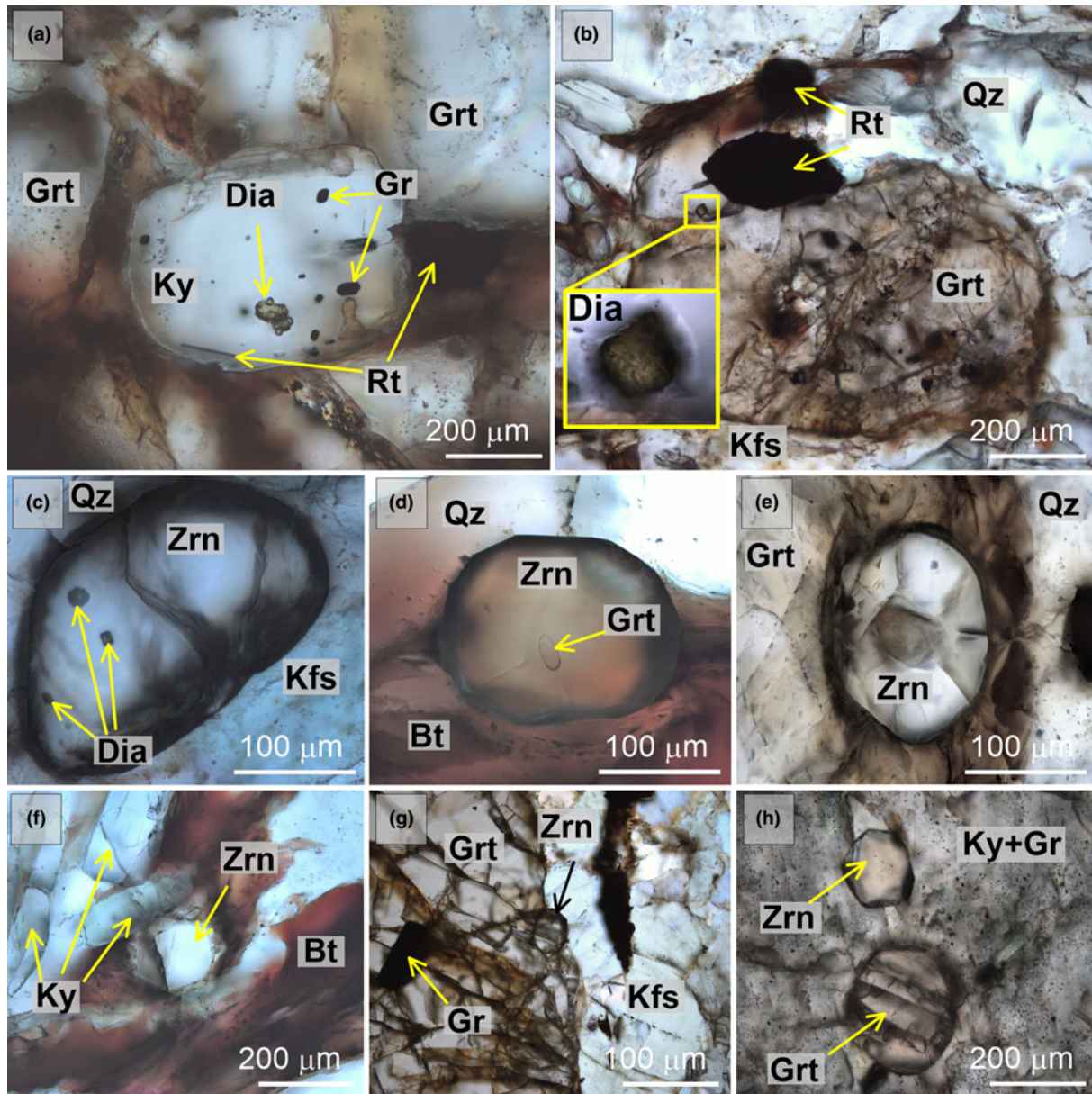


**Fig. 2.** Photomicrographs (transmitted light) of the investigated diamondiferous kyanite gneiss. Diamond was identified as inclusions in kyanite (a), garnet (b) and zircon (c). Zircon occurs in the rock matrix (c,d,f) and as inclusions in garnet (e,g) and kyanite (h). Mineral abbreviations are after (Whitney and Evans, 2010).

and are undetectable in transmitted light, yet they were evidently distinguishable by CL and Raman imaging. This domain shows a moderate CL emission (Fig. 4b), high FWHM values of the  $\nu_3(\text{SiO}_4)$  band ( $11.4\text{--}12.3\text{ cm}^{-1}$ ) (Fig. 4d) and a low

**Table 1.** Experimental parameters for 2D Raman mapping by an Alpha 300 AR confocal Raman microscope

Scan size ( $\mu\text{m}$ )	120 × 140
Resolution (points)	120 × 140
Integration time (s)	0.1
Objective	100 × air (NA 0.75)
Diffraction grating (grids per mm)	600
Excitation wavelength (nm)	488
CCD camera	Back-illuminated CCD 1600×200 pixels (optimised for VIS detection)
Confocal hole ( $\mu\text{m}$ )	50

$\nu_3(\text{SiO}_4)$  peak intensity (Fig. 4e,g). The inner mantles are characterised by lower U (196–242 ppm), Th (below detection limit) and  $\text{HfO}_2$  (up to 1.82 wt.%) concentrations compared with those in the cores, whereas Ti abundance reaches 44 ppm (Table 2).

Domain III represents the outer mantles hosting numerous inclusions of cuboctahedral diamond crystals (up to 20  $\mu\text{m}$ ) with subsidiary coesite, garnet, graphite and rutile (Fig. 4f). In CL images this domain appears as a zone with the highest CL intensity of the recognised domains (Fig. 4b), whereas in the Raman maps of the  $\nu_3(\text{SiO}_4)$  band, Domain III can be identified by the lowest FWHM ( $9.6\text{--}10.5\text{ cm}^{-1}$ ) (Fig. 4d) and the highest peak intensity (Fig. 4e). The main  $\nu_3(\text{SiO}_4)$  band in the Raman spectra of Domain III is clearly shifted to higher wavenumbers (Fig. 4g). The outer mantles also differ from the other domains by the absence of U and Th and the highest

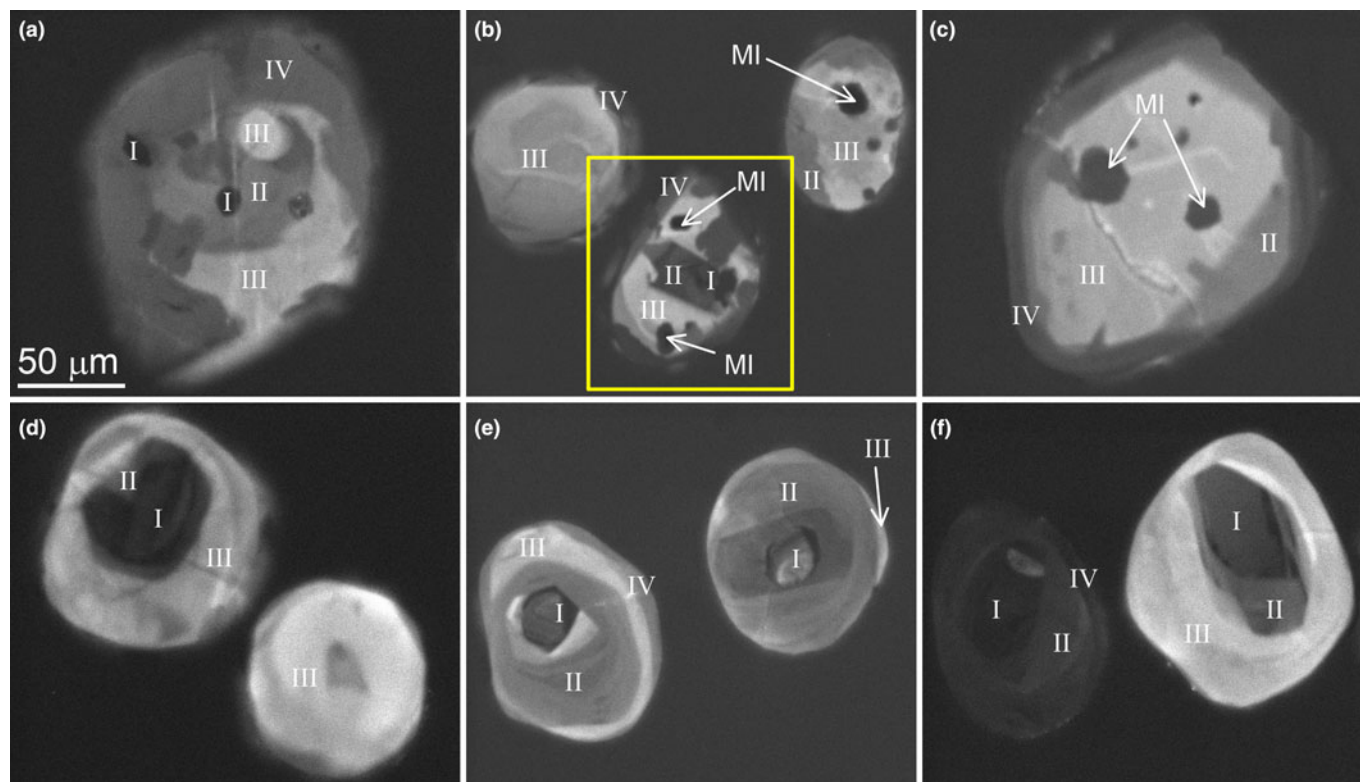


**Fig. 3.** Cathodoluminescence images of zircon with 'spotted' (a) and concentric (b–f) zoning patterns. MI – mineral inclusions, Roman numerals I–IV denote distinct zircon domains. The zircon outlined by a yellow rectangle was selected for 2D Raman mapping.

Ti levels (up to 64 ppm); the  $\text{HfO}_2$  content remains constant compared to the inner mantle (Table 2).

Domain IV constitutes inclusion-free overgrowths of Domain III and can be clearly identified in CL images by a dark signal (Fig. 4b). The Raman maps demonstrate high FWHM ( $13.4\text{--}13.5\text{ cm}^{-1}$ ) (Fig. 4d) and low values of peak intensities of the  $\nu_3(\text{SiO}_4)$  band in this zone (Fig. 4e,g). U and Th contents vary from 97 to 696 ppm and from below detection limit to 447 ppm, respectively. The  $\text{HfO}_2$  content is between 1.62 and 1.89 wt.%. As in Domain I, the Ti abundance in Domain IV is below the limit of detection ( $<12$  ppm) (Table 2).

There is a clear negative correlation between the FWHM of the  $\nu_3(\text{SiO}_4)$  Raman band and its position in the zircon domains (Fig. 5). This relationship has been established recently for zircon inclusions in garnet megablasts from the Dora Maira massif (Campomenosi *et al.*, 2020).

### Raman spectroscopy of diamond included in zircon

The FWHM values and peak position of the main Raman band ( $1332\text{ cm}^{-1}$ ) of the diamond inclusions in zircon vary from 5.8 to 6.8 and from  $1332.5$  to  $1333.5\text{ cm}^{-1}$ , respectively. These values are similar to those obtained previously for diamond crystals from various types of rocks within the Kokchetav massif (Perraki *et al.*, 2009; Shimizu and Ogasawara, 2014; Korsakov *et al.*, 2015). In the FWHM *vs.* peak position plot (Fig. 6), the points form a distinct field that partially overlaps with the data of Perraki *et al.* (2009). Compared to possibly radiation-damaged microdiamond inclusions in zircon cores from tourmaline-rich quartzofeldspathic rock (Shimizu and Ogasawara, 2014), the main Raman peak of the diamonds examined here is generally shifted to higher wavenumbers (Fig. 6). In addition to the main diamond Raman band ( $1332\text{ cm}^{-1}$ ), we have also

**Table 2.** Key characteristics of the distinct zircon domains.

Domain	I	II	III	IV
Position in grain	Centre	Inner mantle	Outer mantle	Rim
CL intensity	Low	Intermediate	High	Low
Intensity of $\nu_3(\text{SiO}_4)$	Extremely low	Low	High	Low
FWHM of $\nu_3(\text{SiO}_4)$ ( $\text{cm}^{-1}$ )	15.5–15.7	11.4–12.3	9.6–10.5	13.4–13.5
Metamict state	Moderately disordered	Mildly disordered	Mildly disordered	Mildly disordered
Ti (ppm)	bdl	Up to 44	Up to 64	bdl
$\text{HfO}_2$ (wt.%)	Up to 2.15	Up to 1.82	Up to 1.82	1.62–1.89
U (ppm)	Up to 1494	196–242	bdl	97–696
Th (ppm)	Up to 115	bdl	bdl	Up to 447
Mineral inclusions	Graphite, quartz	None	Diamond, coesite, garnet, rutile	None

bdl – element concentration is below the detection limit.

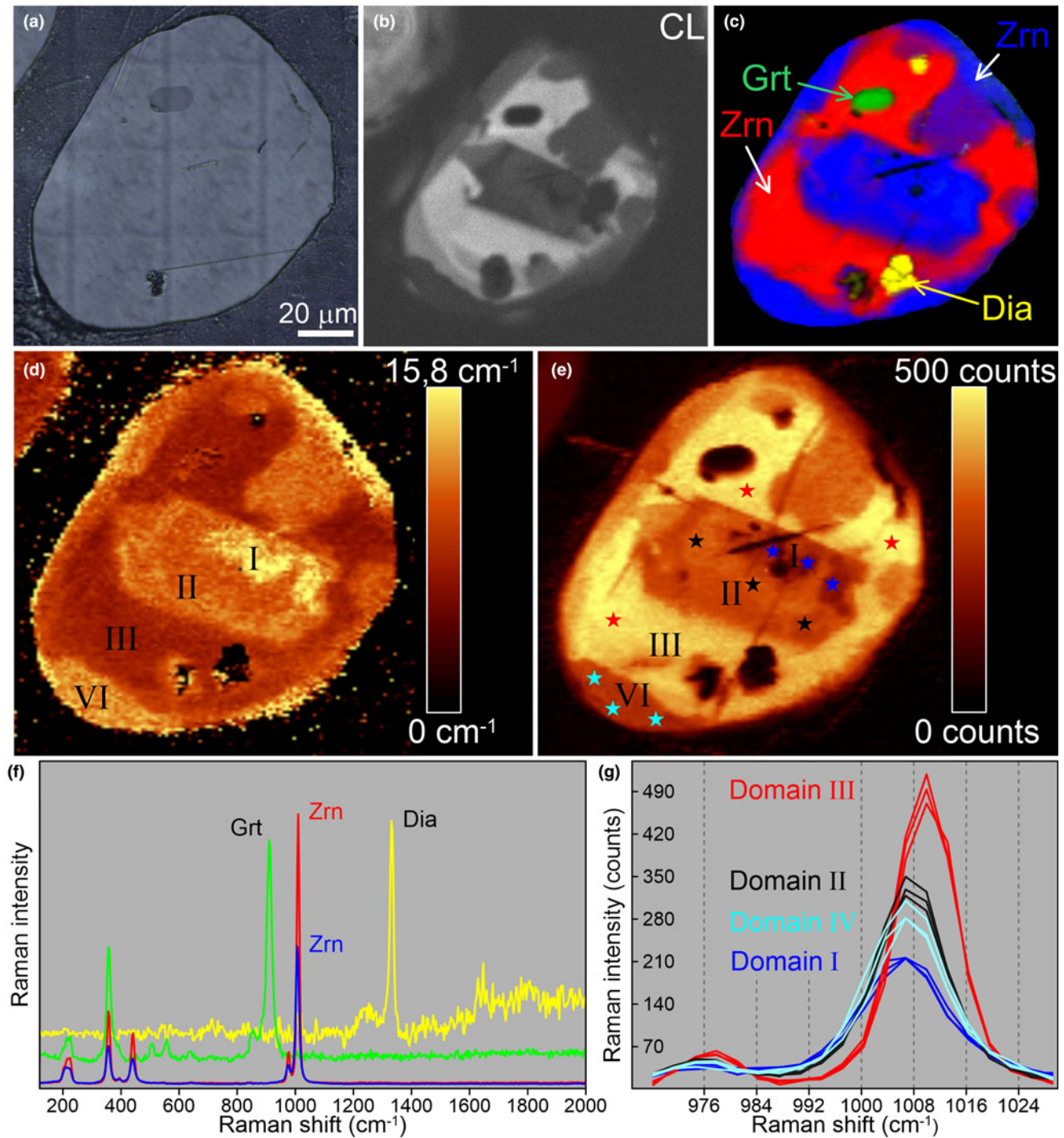


**Fig. 4.** Graphical representation of the analytical data for a representative zircon from the diamondiferous gneiss: (a) reflected-light image, (b) CL image; (c) 2D Raman spectra map showing zircon-hosted inclusions (green, garnet; yellow, diamond; red and blue, host zircon); (d) 2D Raman map of the  $\nu_3(\text{SiO}_4)$  peak full width at half maximum variations ( $\text{cm}^{-1}$ ); (e) 2D Raman map of the  $\nu_3(\text{SiO}_4)$  intensity variations (counts) with star symbols indicating single point Raman measurements; (f) representative Raman spectra of garnet (green) and diamond (yellow) inclusions in the zircon (red and blue); (g) representative Raman spectra of different zircon domains; the colour of each spectrum corresponds to the colour of the stars in (e). Mineral abbreviations are after Whitney and Evans (2010).

identified less intensive peaks at  $\sim 1490 \text{ cm}^{-1}$  and  $\sim 1630 \text{ cm}^{-1}$ . The appearance of the two additional peaks in the diamond Raman spectrum might result from radiation damage of diamond inclusions during  $\alpha$ -particle emission from radioactive decay of U and Th in host zircon (Orwa *et al.*, 2000; Shimizu and Ogasawara, 2014).

## Discussion

The combined application of the CL, Raman spectroscopy and EPMA techniques revealed complex internal zoning patterns of zircon from the diamondiferous kyanite gneisses studied. As a rule, 'spotted' zoning in zircon (Fig. 3a) is hard to interpret, as such zircons contain very few inclusions and the size of distinct

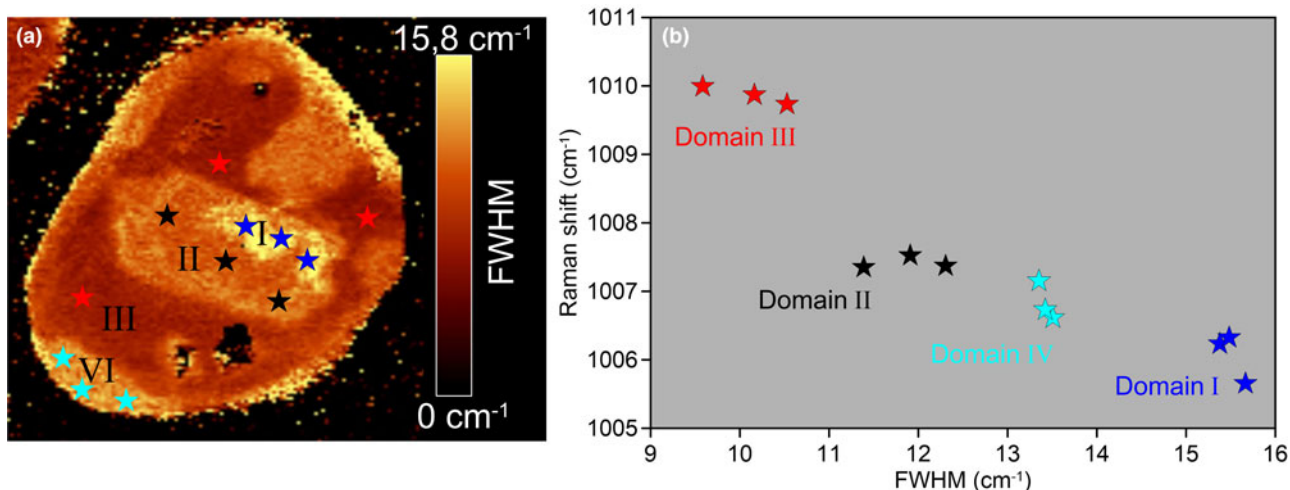


**Fig. 5.** (a) 2D Raman map of the  $\nu_3(\text{SiO}_4)$  peak full width at half maximum variations ( $\text{cm}^{-1}$ ) with star symbols indicating single point Raman measurements; (b) FWHM vs. Raman shift of the  $\nu_3(\text{SiO}_4)$  band ( $\sim 1008 \text{ cm}^{-1}$ ) of different zircon domains. The representative Raman spectra of distinct zircon domains were acquired using an Alpha300 AR confocal Raman microscope (diffraction grating of 600 gr/mm, excitation wavelength = 488 nm)

domains is too small to allow reliable *in situ* isotope-geochemical studies to be performed. By contrast, zircons with concentric zoning are favourable for the reconstruction of their growth stages, as it is possible to obtain temperature estimates for each domain via the application of the Ti-in-zircon geothermometer.

The experimental studies performed at high PT parameters showed Ti content in zircon exhibits a linear dependence on temperature (Watson *et al.*, 2006; Ferry and Watson, 2007). The low Ti concentrations (<12 ppm) in the zircon cores (Domain I) and rims (Domain IV) indicate formation temperatures below 760°C

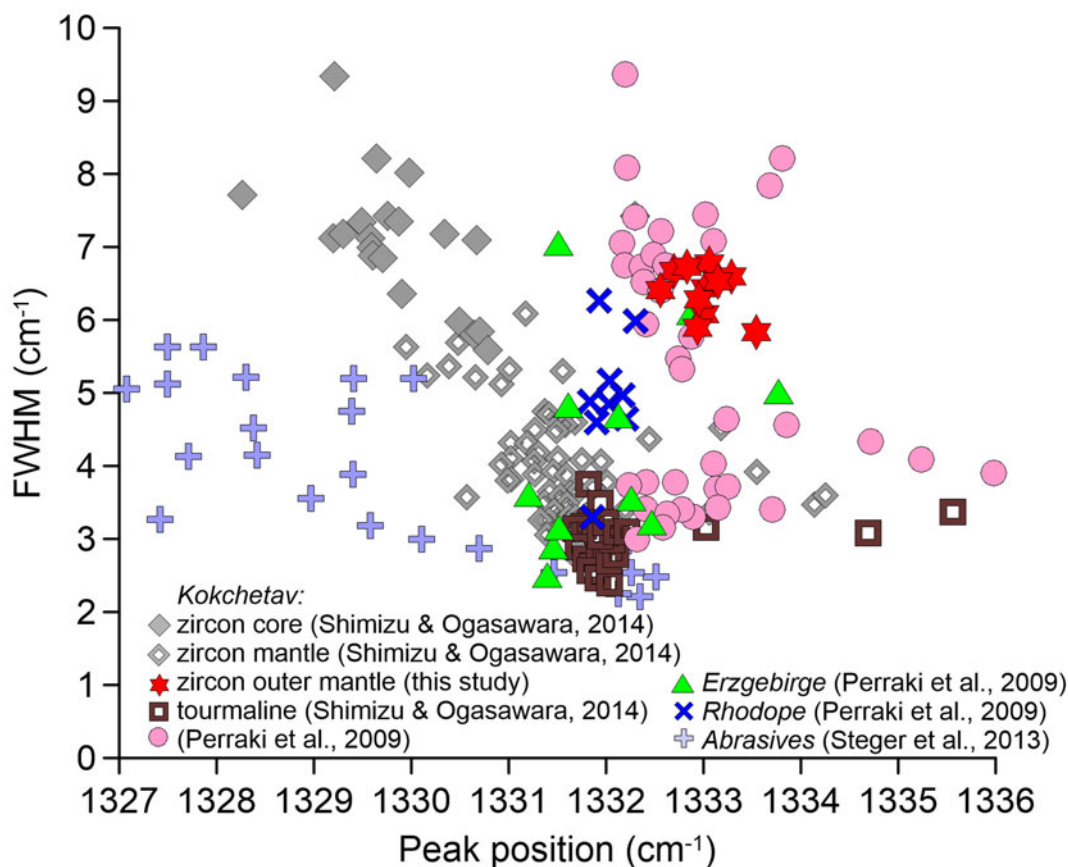


**Fig. 6.** Plots of FWHM vs. peak position of the main Raman band ( $1332 \text{ cm}^{-1}$ ) of microdiamonds. The occurrence (host mineral) of microdiamond is indicated in the legend.

using the Ti-in-zircon geothermometer of Ferry and Watson (2007). The temperatures obtained for the inner inclusion-free mantles (Domain II) range from 760 to 880°C, whereas for the diamond-bearing outer mantles (Domain III) the temperatures are  $900 \pm 30^\circ\text{C}$ .

Note, however, that the Ti-in-zircon geothermometer is based on an experimental data set at pressures of  $\sim 1$  GPa. At higher pressures (e.g. those required for the formation of the diamond-grade kyanite gneisses examined here) this geothermometer is known to give overestimated temperature values (Tailby *et al.*, 2011; Stepanov *et al.*, 2016b). The Zr-in-rutile geothermometer based on the solubility of  $\text{ZrO}_2$  in rutile coexisting with zircon and quartz is also extensively applied to estimate peak metamorphic temperatures (Watson *et al.*, 2006; Ferry and Watson, 2007; Tomkins *et al.*, 2007). A study of pressure dependence of the Zr-in-rutile geothermometer revealed that a correction of temperature values is needed at pressures exceeding 4 GPa (Tomkins *et al.*, 2007; Stepanov *et al.*, 2016b). Taking into account the corrections proposed by Stepanov *et al.* (2016b) for UHP conditions, high Zr contents in rutile grains from the kyanite gneisses studied (up to 900 ppm) yield temperature values of  $900 \pm 30^\circ\text{C}$  (for 5 GPa).

In the following discussion we reconcile the temperature estimates obtained with the inclusion mineralogy within particular zircon domains and literature data. The first detailed studies of zircons from the Kokchetav UHPM rocks were performed  $\sim 30$  years ago (Claoué-Long *et al.*, 1991; Sobolev *et al.*, 1991). Zircon cores from biotite-garnet diamondiferous gneiss with radiometric ages of ca. 1981 Ma were interpreted as being of detrital or pre-metamorphic origin (Claoué-Long *et al.*, 1991). Subsequently, Katayama *et al.* (2000, 2001), Hermann *et al.* (2001), and Stepanov *et al.* (2016b) supported this suggestion by a study of inclusions of LP minerals in inherited zircon cores from diamondiferous rocks of the Kokchetav massif. The presence of oscillatory zoning in zircon is commonly regarded as a signature of magmatic origin (e.g. Corfu *et al.*, 2003; Wu and Zheng, 2004); such zoning patterns have also been observed in this study (Fig. 3e). In contrast, some zircon cores from the diamondiferous Kokchetav rocks described by Katayama *et al.* (2001) and Shimizu and Ogasawara (2014) contain microdiamonds, indicating formation of these cores under UHP conditions. Generally, zircon cores from Kokchetav diamondiferous rocks have ages of 520–1981 Ma (Claoué-Long *et al.*, 1991; Katayama *et al.*, 2001; Hermann *et al.*, 2006; Stepanov *et al.*, 2016b); however, Rubatto and Hermann (2007) proposed that the cores could be “isotopically disturbed” and thus had yielded unreliable ages. There is also an issue of radiometric age determination accuracy for relatively old metamorphic rocks, namely that the ages of distinct metamorphic stages overlap within the value of radiometric age determination uncertainty (Rubatto *et al.*, 2003; Hermann *et al.*, 2006).

Nevertheless, the zircon cores examined here (Domain I) appear to be of detrital origin, which is inferred from their low Ti abundances, inclusions of LP minerals and oscillatory zoning patterns. Katayama *et al.* (2000) and Hermann *et al.* (2001) showed that zircon cores are surrounded by mantles with coesite and diamond inclusions providing evidence for the UHP formation of the mantles. In our study, the inherited (probably magmatic) zircon cores (Domain I) are surrounded by the inclusion-free inner mantles (Domain II), which, however, have relatively high Ti contents (up to 40 ppm) testifying to their formation at the temperatures up to 880°C, i.e. during the prograde

metamorphic stage. Some zircon grains do not contain cores (Domain I) or inner mantles (Domain II), which can be explained by different grain size, and, therefore, different cross-section depth.

However, the inclusions of UHP mineral indicators, coesite and diamond, were identified in the outer mantles (Domain III) and unambiguously indicate that the outer mantles crystallised near the peak metamorphic conditions. The temperature estimates obtained using the Ti-in-zircon geothermometer for Domain III ( $900 \pm 30^\circ\text{C}$ ) are consistent with those afforded by the Zr-in-rutile geothermometer for the diamondiferous rocks of the Kokchetav massif ( $900 \pm 30^\circ\text{C}$ ; Stepanov *et al.*, 2016b), which further proves the outer mantles of the zircon grains to have been formed near the peak of metamorphism.

Finally, the low Ti content in the zircon rims (Domain IV), as well as the absence of diamond/coesite inclusions in this zone, probably indicates their formation on the retrograde metamorphic stage during exhumation and cooling (Stepanov *et al.*, 2016a). This conclusion is convincingly supported by the U–Pb ages of Kokchetav zircon rims that are much younger than the peak of metamorphism (Hermann *et al.*, 2001; Katayama *et al.*, 2001).

## Summary

The comparison of CL and Raman spectroscopy data revealed that the discrete zircon domains detected in the CL images are reproduced clearly in the Raman maps of the  $1008\text{ cm}^{-1}$  peak FWHM and position. Hence, zircon internal textures can also be deciphered by Raman spectroscopy, especially for the case of unexposed zircon grains, whose study by CL methods is impossible. The evidence we have obtained on the complex internal zircon texture implies a close genetic link between the observed zircon domains and episodes of its growth. The heterogeneity of the zircon interior together with the distribution of mineral inclusions in individual domains implies multi-stage crystallisation. The cores (Domain I) are of pre-metamorphic (magmatic) origin ( $<760^\circ\text{C}$ ), inner mantles (Domain II) were formed during the prograde metamorphic stage ( $760\text{--}880^\circ\text{C}$ ), diamond-bearing outer mantles (Domain III) crystallised near the peak metamorphic conditions ( $900 \pm 30^\circ\text{C}$ ), and rims (Domain IV) were formed during the retrograde stage ( $<760^\circ\text{C}$ ). The combined application of CL, Raman spectroscopy and EPMA techniques to zircon is thus regarded as a powerful approach in revealing distinct growth events recorded by this unique mineral.

**Acknowledgements.** This work was performed within the IGM SB RAS and IGG UB RAS (No. AAAA-A19-119071090011-6) state assignment projects. Financial support was provided by RFBR project no. 19-35-90002. D.I.R. was supported by the research grant program of the President of the Russian Federation for young Russian scientists (MK-971.2020.5). The equipment of the Ural Centre for Shared Use “Modern Nanotechnologies”, Ural Federal University, and the Common Use Centre of the Ural Branch of RAS “Geoanalyst” was used. We thank journal editor Roger Mitchell for efficient handling of the manuscript and Tatsuki Tsujimori and an anonymous reviewer for their helpful comments and suggestions that improved the quality of the report.

## References

- Buslov M.M., Dobretsov N.L., Vovna G.M. and Kiselev V.I. (2015) Structural location, composition, and geodynamic nature of diamond-bearing metamorphic rocks of the Kokchetav subduction-collision zone of the Central

- Asian Fold Belt (northern Kazakhstan). *Russian Geology and Geophysics*, **56**, 64–80.
- Caruba R., Baumer A., Ganteaume M. and Iacconi P. (1985) An experimental study of hydroxyl groups and water in synthetic and natural zircons: a model of the metamict state. *American Mineralogist*, **70**, 1224–1231.
- Campomenosi N., Rubatto D., Hermann J., Mihailova B., Scambelluri M. and Alvaro M. (2020) Establishing a protocol for the selection of zircon inclusions in garnet for Raman thermobarometry. *American Mineralogist: Journal of Earth and Planetary Materials*, **105**, 992–1001.
- Chakoumakos B.C., Murakami T., Lumpkin G.R. and Ewing R.C. (1987) Alpha-decay-induced fracturing in zircon: the transition from the crystalline to the metamict state. *Science*, **236**, 1556–1559.
- Chopin C. and Sobolev N.V. (1995) Principal mineralogical indicators of UHP in crustal rocks. Pp. 96–131 in: *Ultra-high-Pressure Metamorphism* (R.G. Coleman and X. Wang, editors). Cambridge University Press, UK.
- Claoué-Long J.C., Sobolev N.V., Shatsky V.S. and Sobolev A.V. (1991) Zircon response to diamond-pressure metamorphism in the Kokchetav massif, USSR. *Geology*, **19**, 710–713.
- Corfu F., Hanchar J.M., Hoskin P.W.O. and Kinny P. (2003) Atlas of zircon textures. Pp. 469–500 in: *Zircon* (J.M. Hanchar and P.W.O. Hoskin, editors). Reviews in Mineralogy and Geochemistry, **53**. Mineralogical Society of America and the Geochemical Society, Chantilly, Virginia, USA.
- Dobretsov N.L. (1998) Structural and geodynamic evolution of diamond-bearing metamorphic rocks of Kokchetav Massif, Kazakhstan. *Russian Geology and Geophysics*, **39**, 1650–1661.
- Dobretsov N.L. and Shatsky V.S. (2004) Exhumation of high-pressure rocks of the Kokchetav massif: facts and models. *Lithos*, **78**, 307–318.
- Dobretsov N.L., Shatsky V.S. and Sobolev N.V. (1995a) Comparison of the Kokchetav and Dabie Shan metamorphic complexes: coesite- and diamond-bearing rocks and UHP-HP accretional-collisional events. *International Geology Review*, **37**, 636–656.
- Dobretsov N.L., Sobolev N.V., Shatsky V.S., Coleman R.G. and Ernst W.G. (1995b) Geotectonic evolution of diamondiferous paragneisses, Kokchetav Complex, northern Kazakhstan: The geologic enigma of ultrahigh-pressure crustal rocks within a Paleozoic foldbelt. *Island Arc*, **4**, 267–279.
- Dobretsov N.L., Buslov M.M., Zhimulev F.I., Travin A.V. and Zayachkovsky A.A. (2006) Vendian-Early Ordovician geodynamic evolution and model for exhumation of ultrahigh- and high-pressure rocks from the Kokchetav subduction-collision zone (northern Kazakhstan). *Russian Geology and Geophysics*, **47**, 424–440.
- Ewing R.C., Meldrum A., Wang L., Weber W.J. and Corrales L.R. (2003) Radiation effects in zircon. Pp. 387–425 in: *Zircon* (J.M. Hanchar and P.W.O. Hoskin, editors). Reviews in Mineralogy and Geochemistry, **53**. Mineralogical Society of America and the Geochemical Society, Chantilly, Virginia, USA.
- Farges F. and Calas G. (1991) Structural analysis of radiation damage in zircon and thorite: An X-ray absorption spectroscopic study. *American Mineralogist*, **76**, 60–73.
- Ferry J.M. and Watson E.B. (2007) New thermodynamic models and revised calibrations for the Ti-in-zircon and Zr-in-rutile thermometers. *Contributions to Mineralogy and Petrology*, **154**, 429–437.
- Hacker B.R., Calvert A., Zhang R.Y., Ernst W.G. and Liou J.G. (2003) Ultrarapid exhumation of ultrahigh-pressure diamond-bearing metasedimentary rocks of the Kokchetav Massif, Kazakhstan? *Lithos*, **70**, 61–75.
- Hanchar J.M. and Miller C.F. (1993) Zircon zonation patterns as revealed by cathodoluminescence and backscattered electron images: implications for interpretation of complex crustal histories. *Chemical Geology*, **110**, 1–13.
- Hermann J., Rubatto D., Korsakov A.V. and Shatsky V.S. (2001) Multiple zircon growth during fast exhumation of diamondiferous, deeply subducted continental crust (Kokchetav Massif, Kazakhstan). *Contributions to Mineralogy and Petrology*, **141**, 66–82.
- Hermann J., Rubatto D., Korsakov A. and Shatsky V.S. (2006) The age of metamorphism of diamondiferous rocks determined with SHRIMP dating of zircon. *Russian Geology and Geophysics*, **47**, 513–520.
- Katayama I., Zayachkovsky A.A. and Maruyama S. (2000) Prograde pressure-temperature records from inclusions in zircons from ultrahigh-pressure-high-pressure rocks of the Kokchetav Massif, northern Kazakhstan. *Island Arc*, **9**, 417–427.
- Katayama I., Maruyama S., Parkinson C.D., Terada K. and Sano Y. (2001) Ion micro-probe U–Pb zircon geochronology of peak and retrograde stages of ultrahigh-pressure metamorphic rocks from the Kokchetav massif, northern Kazakhstan. *Earth and Planetary Science Letters*, **188**, 185–198.
- Katayama I., Muko A., Iizuka T., Maruyama S., Terada K., Tsutsumi Y., Sano Y., Zhang R.Y. and Liou J.G. (2003) Dating of zircon from Ti-clinohumite-bearing garnet peridotite: Implication for timing of mantle metasomatism. *Geology*, **31**, 713–716.
- Katayama I. and Maruyama S. (2009) Inclusion study in zircon from ultrahigh-pressure metamorphic rocks in the Kokchetav massif: an excellent tracer of metamorphic history. *Journal of the Geological Society*, **166**, 783–796.
- Korsakov A.V., Shatsky V.S., Sobolev N.V. and Zayachkovsky A.A. (2002) Garnet-biotite-clinozoisite gneiss: a new type of diamondiferous metamorphic rock from the Kokchetav Massif. *European Journal of Mineralogy*, **14**, 915–928.
- Korsakov A.V., Toporski J., Dieing T., Yang J. and Zelenovskiy P.S. (2015) Internal diamond morphology: Raman imaging of metamorphic diamonds. *Journal of Raman Spectroscopy*, **46**, 880–888.
- Liao J., Malusà M.G., Zhao L., Baldwin S.L., Fitzgerald P.G. and Gerya T. (2018) Divergent plate motion drives rapid exhumation of (ultra) high pressure rocks. *Earth and Planetary Science Letters*, **491**, 67–80.
- Liou J.G., Tsujimori T., Yang J., Zhang R.Y. and Ernst W.G. (2014) Recycling of crustal materials through study of ultrahigh-pressure minerals in collisional orogens, ophiolites, and mantle xenoliths: A review. *Journal of Asian Earth Sciences*, **96**, 386–420.
- Liu F.L. and Liou J.G. (2011) Zircon as the best mineral for P–T–time history of UHP metamorphism: a review on mineral inclusions and U–Pb SHRIMP ages of zircons from the Dabie–Sulu UHP rocks. *Journal of Asian Earth Sciences*, **40**, 1–39.
- Marsellos A.E. and Garver J.I. (2010) Radiation damage and uranium concentration in zircon as assessed by Raman spectroscopy and neutron irradiation. *American Mineralogist*, **95**, 1192–1201.
- Mikhno A.O. and Korsakov A.V. (2013) K<sub>2</sub>O prograde zoning pattern in clinopyroxene from the Kokchetav diamond-grade metamorphic rocks: Missing part of metamorphic history and location of second critical end point for calc-silicate system. *Gondwana Research*, **23**, 920–930.
- Mikhno A.O. and Korsakov A.V. (2015) Carbonate, silicate, and sulfide melts: heterogeneity of the UHP mineral-forming media in calc-silicate rocks from the Kokchetav massif. *Russian Geology and Geophysics*, **56**, 81–99.
- Mosenfelder J.L., Schertl H.-P., Smyth J.R. and Liou J.G. (2005) Factors in the preservation of coesite: The importance of fluid infiltration. *American Mineralogist*, **90**, 779–789.
- Murakami T., Chakoumakos B.C. and Ewing R.C. (1986) X-ray powder diffraction analysis of alpha-event radiation damage in zircon (ZrSiO<sub>4</sub>). Pp. 745–753 in: *Advances in Ceramics: Nuclear Waste Management II* (D.E. Clark, W.B. White and J. Machiels, editors). American Ceramic Society, Columbus, Ohio.
- Nasdala L., Irmer G. and Wolf D. (1995) The degree of metamictization in zircons: a Raman spectroscopic study. *European Journal of Mineralogy*, **7**, 471–478.
- Nasdala L., Wenzel M., Vavra G., Irmer G., Wenzel T. and Kober B. (2001) Metamictisation of natural zircon: accumulation versus thermal annealing of radioactivity-induced damage. *Contributions to Mineralogy and Petrology*, **141**, 125–144.
- Nasdala L., Lengauer C.L., Hanchar J.M., Kronz A., Wirth R., Blanc P., Kennedy A.K. and Seydoux-Guillaume A.-M. (2002) Annealing radiation damage and the recovery of cathodoluminescence. *Chemical Geology*, **191**, 121–140.
- Nasdala L., Kronz A., Hanchar J.M., Tichomirowa M., Davis D.W. and Hofmeister W. (2006) Effects of natural radiation damage on back-scattered electron images of single crystals of minerals. *American Mineralogist*, **91**, 1739–1746.
- Ogasawara Y., Fukasawa K. and Maruyama S. (2002) Coesite exsolution from supersilicic titanite in UHP marble from the Kokchetav Massif, northern Kazakhstan. *American Mineralogist*, **87**, 454–461.

- Orwa J.O., Nugent K.W., Jamieson D.N. and Prawer S. (2000) Raman investigation of damage caused by deep ion implantation in diamond. *Physical Review B*, **62**, 5461.
- Ota T., Terabayashi M., Parkinson C.D. and Masago H. (2000) Thermobaric structure of the Kokchetav ultrahigh-pressure–high-pressure massif deduced from a north–south transect in the Kulet and Saldat–Kol regions, northern Kazakhstan. *Island Arc*, **9**, 328–357.
- Palenik C.S., Nasdala L. and Ewing R.C. (2003) Radiation damage in zircon. *American Mineralogist*, **88**, 770–781.
- Parkinson C.D. (2000) Coesite inclusions and prograde compositional zonation of garnet in whiteschist of the HP-UHPM Kokchetav massif, Kazakhstan: a record of progressive UHP metamorphism. *Lithos*, **52**, 215–233.
- Parkinson C.D. and Katayama I. (1999) Present-day ultrahigh-pressure conditions of coesite inclusions in zircon and garnet: Evidence from laser Raman microspectroscopy. *Geology*, **27**, 979–982.
- Perchuk L.L., Safonov O.G., Yapaskurt V.O. and Barton Jr J.M. (2002) Crystal-melt equilibria involving potassium-bearing clinopyroxene as indicator of mantle-derived ultrahigh-potassic liquids: an analytical review. *Lithos*, **60**, 89–111.
- Perraki M., Korsakov A.V., Smith D.C. and Mposkos E. (2009) Raman spectroscopic and microscopic criteria for the distinction of microdiamonds in ultrahigh-pressure metamorphic rocks from diamonds in sample preparation materials. *American Mineralogist*, **94**, 546–556.
- Rubatto D. and Hermann J. (2007) Zircon behaviour in deeply subducted rocks. *Elements*, **3**, 31–35.
- Rubatto D., Liati A. and Gebauer D. (2003) *Dating UHP metamorphism*. Pp. 341–363 in: EMU Notes in Mineralogy, Vol. 5.
- Schaltegger U., Fanning C.M., Günther D., Maurin J.C., Schulmann K. and Gebauer D. (1999) Growth, annealing and recrystallization of zircon and preservation of monazite in high-grade metamorphism: conventional and in-situ U-Pb isotope, cathodoluminescence and microchemical evidence. *Contributions to Mineralogy and Petrology*, **134**, 186–201.
- Schertl H.-P. and Sobolev N.V. (2013) The Kokchetav Massif, Kazakhstan: “Type locality” of diamond-bearing UHP metamorphic rocks. *Journal of Asian Earth Sciences*, **63**, 5–38.
- Shatsky V.S., Sobolev N.V., Zayachkovsky A.A., Zorin T.Y. and Vavilov M.A. (1991) New occurrence of microdiamonds in metamorphic rocks as a proof of regional character of ultrahigh pressure metamorphism in Kokchetav massif. *Doklady Akademii Nauk SSSR*, **321**, 193–198.
- Shatsky V.S., Theunissen K., Dobretsov N.L. and Sobolev N.V. (1998) New indications of ultrahigh-pressure metamorphism in the mica schists of the Kulet site of the Kokchetav Massif (north Kazakhstan). *Russian Geology and Geophysics*, **39**, 1041–1046.
- Shatsky V.S., Jagoutz E., Sobolev N.V., Kozmenko O.A., Parkhomenko V.S. and Troesch M. (1999) Geochemistry and age of ultrahigh pressure metamorphic rocks from the Kokchetav massif (Northern Kazakhstan). *Contributions to Mineralogy and Petrology*, **137**, 185–205.
- Shatsky V.S., Skuzovatov S.Y., Ragozin A.L. and Sobolev N.V. (2015) Mobility of elements in a continental subduction zone: evidence from the UHP metamorphic complex of the Kokchetav massif. *Russian Geology and Geophysics*, **56**, 1016–1034.
- Shchepetova O.V., Korsakov A.V., Mikhailenko D.S., Zelenovskiy P.S., Shur V.Y. and Ohfuji H. (2017) Forbidden mineral assemblage coesite-disordered graphite in diamond-bearing kyanite gneisses (Kokchetav Massif). *Journal of Raman Spectroscopy*, **48**, 1606–1612.
- Shimizu N. (1971) Potassium contents of synthetic clinopyroxenes at high pressures and temperatures. *Earth and Planetary Science Letters*, **11**, 374–380.
- Shimizu R. and Ogasawara Y. (2014) Radiation damage to Kokchetav UHPM diamonds in zircon: Variations in Raman, photoluminescence, and cathodoluminescence spectra. *Lithos*, **206**, 201–213.
- Sobolev N.V. (1994) Zircon from ultrahigh pressure metamorphic rocks of folded regions as an unique container of inclusions of diamond, coesite and coexisting minerals. *Doklady Akademii Nauk*, **334**, 488–492.
- Sobolev N.V. and Shatsky V.S. (1990) Diamond inclusions in garnets from metamorphic rocks: a new environment for diamond formation. *Nature*, **343**, 742.
- Sobolev N.V., Shatsky V.S., Vavilov M.A. and Goryainov S.V. (1991) Coesite inclusion in zircon from diamondiferous gneiss of Kokchetav massif—first find of coesite in metamorphic rocks in the USSR territory. *Doklady Akademii Nauk SSSR*, **321**, 184–188.
- Steger S., Nasdala L. and Wagner A. (2013) *Raman spectra of diamond abrasives and possible artefacts in detecting UHP microdiamond*. CORALS–2013 (Conference on Raman and Luminescence Spectroscopy in the Earth Sciences), Vienna, Austria, pp. 95–96.
- Stepanov A.S., Hermann J., Rubatto D., Korsakov A.V. and Danyushevsky L.V. (2016a) Melting history of an ultrahigh-pressure paragneiss revealed by multiphase solid inclusions in garnet, Kokchetav massif, Kazakhstan. *Journal of Petrology*, **57**, 1531–1554.
- Stepanov A.S., Rubatto D., Hermann J. and Korsakov A.V. (2016b) Contrasting PT paths within the Barchi-Kol UHP terrain (Kokchetav Complex): Implications for subduction and exhumation of continental crust. *American Mineralogist*, **101**, 788–807.
- Tailby N.D., Walker A.M., Berry A.J., Hermann J., Evans K.A., Mavrogenes J.A., O'Neill H.S.C., Rodina I.S., Soldatov A.V. and Rubatto D. (2011) Ti site occupancy in zircon. *Geochimica et Cosmochimica Acta*, **75**, 905–921.
- Theunissen K., Dobretsov N.L., Korsakov A.V., Travin A.V., Shatsky V.S., Smirnova L.V. and Boven A. (2000) Two contrasting petrotectonic domains in the Kokchetav megamelange (north Kazakhstan): difference in exhumation mechanisms of ultrahigh-pressure crustal rocks, or a result of subsequent deformation? *Island Arc*, **9**, 284–303.
- Tomkins H.S., Powell R. and Ellis D.J. (2007) The pressure dependence of the zirconium-in-rutile thermometer. *Journal of Metamorphic Geology*, **25**, 703–713.
- Vavra G. (1990) On the kinematics of zircon growth and its petrogenetic significance: a cathodoluminescence study. *Contributions to Mineralogy and Petrology*, **106**, 90–99.
- Watson E.B., Wark D.A. and Thomas J.B. (2006) Crystallization thermometers for zircon and rutile. *Contributions to Mineralogy and Petrology*, **151**, 413.
- Weber W.J., Ewing R.C. and Meldrum A. (1997) The kinetics of alpha-decay-induced amorphization in zircon and apatite containing weapons-grade plutonium or other actinides. *Journal of Nuclear Materials*, **250**, 147–155.
- Whitney D.L. and Evans B.W. (2010) Abbreviations for names of rock-forming minerals. *American Mineralogist*, **95**, 185–187.
- Woodhead J.A., Rossman G.R. and Silver L.T. (1991) The metamictization of zircon: Radiation dose-dependent structural characteristics. *American Mineralogist*, **76**, 74–82.
- Wu Y. and Zheng Y. (2004) Genesis of zircon and its constraints on interpretation of U-Pb age. *Chinese Science Bulletin*, **49**, 1554–1569.
- Zamyatin D.A., Shchapova Y.V., Votyakov S.L., Nasdala L. and Lenz C. (2017) Alteration and chemical U-Th-total Pb dating of heterogeneous high-uranium zircon from a pegmatite from the Aduiskii Massif, Middle Urals, Russia. *Mineralogy and Petrology*, **111**, 475–497.
- Zamyatin D.A., Votyakov S.L. and Shchapova Y.V. (2019) JPD-analysis as a new approach for studying the zircon texture with micron spatial resolution with application to geochronology. *Doklady Earth Sciences*, **485**, 376–380.
- Zhang M. and Salje E.K.H. (2001) Infrared spectroscopic analysis of zircon: Radiation damage and the metamict state. *Journal of Physics: Condensed Matter*, **13**, 3057.
- Zhang M., Salje E.K.H., Ewing R.C., Farnan I., Ríos S., Schlüter J. and Leggo P. (2000) Alpha-decay damage and recrystallization in zircon: evidence for an intermediate state from infrared spectroscopy. *Journal of Physics: Condensed Matter*, **12**, 5189.
- Zhang R.Y., Liou J.G., Ernst W.G., Coleman R.G., Sobolev N.V. and Shatsky V.S. (1997) Metamorphic evolution of diamond-bearing and associated rocks from the Kokchetav Massif, northern Kazakhstan. *Journal of Metamorphic Geology*, **15**, 479–496.